Electronic Supplementary Information

Templated nanoreactors array toward nanoscale-tunable liquid-phase catalysis

Shuo Zhang, Xie Quan,* Shuo Chen and Hongtao Yu

Key Laboratory of Industrial Ecology and Environmental Engineering (MOE), School of Environmental Science and Technology, Dalian University of Technology, Linggong Road 2, Dalian 116024, China. E-mail: quanxie@dlut.edu.cn

Experimental Section

Materials and reagents. Double-pass anodized aluminum oxide (AAO) in thickness of 70 μm was supplied by Hefei Pu-Yuan Nano Technology Co. Ltd. (China). N-methyl-pyrrolidone (≥99%, AR), zinc acetate dihydrate (≥99%, AR), methanol (≥99.5%, AR), ethanol (≥99.7%, AR) were purchased from Damao Chemical Reagent Co. Ltd. (Tianjin, China). Cetytrimethylammonium bromide (≥99%, AR) and benzaldehyde (≥98.5, AR) were supplied by Sinopharm Chemical Reagent Co. Ltd. (Shanghai, China). Malononitrile (99%) was purchased from Aladdin Industrial Corporation (Shanghai, China). Benzylidenemalononitrile (＞98%) was purchased from TCI Development Co. Ltd. (Shanghai, China). There was no further purification of all the chemicals used in this work.

Templated synthesis of nanoreactors. Arrayed nanostructures were synthesized via AAO-templated solvothermal processes using sol-gel precursors. In a typical procedure, cetytrimethylammonium bromide (CTAB) of 0.016 M were added in 20 mL of N-methyl-pyrrolidone (NMP) as a mixture solvent. Organic precursors, i.e., zinc acetate for zinc oxide nanotubes (Fig. 1a), ferrous chloride for iron oxide nanoplates (Fig. 1b), manganese acetate for manganese oxide (Fig. 1c), and cerium nitrate for cerium oxide nanobrushes (Fig. 1d), were added to the mixture matrix and ultrasonically treated for 25 min at 65 °C. Upon the formation of uniform sol, the prepared mixtures were placed in a Teflon-lined autoclave, together with AAO template

(200-300 nm pore) immersed at the middle of the vessel. The sealed autoclave was heated to 180 °C for 4 h and cooled down naturally at ambient temperature. Ultrasound was used to wash the surface of AAO-templated material in absolute ethanol environment. Afterwards, it was placed in a 40 °C oven for 1 h and then underwent a 2 h heating at 400 °C. Finally, the arrayed nanostructures were obtained.

Characterization. Material morphologies were examined by scanning electron microscopy (SEM) (S4800, Hitachi, Japan) and high-resolution transmission electron microscopy (HRTEM) (JEM-2000EX, Japan). Energy dispersive spectrometer (EDS) was obtained using field emission scanning electron microscope (NOVA NanoSEM 450, FEI, USA). DX-3000 X-ray diffractometer (Shimadzu, Japan) was employed to report X-ray diffraction (XRD) results, for which Cu Kα monochromatic radiation was operated at 40 kV and 100 mA. Chemical composition of zinc oxide was examined by X-ray photoelectron spectroscopy (XPS) using Thermo Fisher XPS instrument (Escalab 250Xi, USA). CheBET Pulsar TPD Analyzer (Quantachrome, USA) was used to acquire temperature-programmed desorption profiles of ammonia (NH_3-TPD) and carbon dioxide (CO_2-TPD), respectively. Autosorb-iQ-C (Quantachrome, USA) was used for a measurement of nitrogen adsorption-desorption isotherms (-196.15 °C). The leaching of Zn^{2+} ions was detected by inductively coupled plasma mass spectrometry (Nex ION 300D, PerkinElmer, USA).

Catalytic reactions in ZnO_{NTs}. Reactions were performed in a two-pass reaction module (Fig. S4). The AAO-templated material was fixed on top of a perforated support and a rubber pad was inserted for a seal. For Knoevenagel condensation, ethanol matrix containing benzaldehyde and malononitrile in equimolar concentrations (13.5 mM) was prepared and stored in the feed tank. In a typical experiment, the mixture solution was first heated to designated temperature by a thermostat, then pumped into the module to initiate catalytic reaction, and permeate liquid was periodically collected and analyzed. The whole reaction system was placed in an oven to maintain the reaction temperature. The product benzylidenemalononitrile (BM) was detected by HPLC (Waters 2695 Separations Module) at wavelength of 221 nm with an eluent solution mixed by ultrapure water (30%) and methanol (70%) at a flowrate of 0.8 mL/min, using SunFire® C18 column (250 mm × 4.6 mm × 5 μm) as the stationary phase.

Determination of retention time (t_R). The time spent for passage of solution in arrayed nanotubes closely correlates with the pore size, arrangement, as well as the liquid flux. After a collection of diameters of the pores (labeled as d_i) according to selected SEM region, the total porous area for passage of solution (S_p, m^2) can be determined according to Equation (S1),

$$s_p = \frac{A_0}{A_{SEM}} \cdot \sum_{i=1}^{n} d_i^2 \cdot \frac{\pi}{4} \tag{S1}$$

where A_0 is the actual exposed area of ZnO_{NT} array for passage of solution, m^2; A_{SEM} is the total area of selected SEM image for collection of d_i, m^2; n is the total number of pores recorded in the selected SEM image, dimensionless.

If the flux is controlled at Q (mL min^{-1}), the t_R (s) can be expressed as

$$t_R = \frac{s_p \cdot \delta \cdot 6 \cdot 10^{-5}}{Q}$$

(S2)

where δ is the thickness of ZnO_{NT}/AAO composite, m.

Specifically, for tests on 168-ZnO_{NT}, flow rates were controlled at 1.0×10^{-4}, 1.5×10^{-4}, 3.0×10^{-4}, 5.0×10^{-4}, and 1.5×10^{-3} L min^{-1} respectively, for which the corresponding t_R were respectively 0.61, 0.41, 0.20, 0.12, 0.04 s; for tests on pore size effect, the values of t_R were controlled at 0.122 s for 168-ZnO_{NT} (flow rate: 5.0×10^{-4} L min^{-1}), 0.119 s for 96-ZnO_{NT} (flow rate: 3.0×10^{-4} L min^{-1}), 0.099 s for 61-ZnO_{NT} (flow rate: 3.0×10^{-4} L min^{-1}), 0.109 s for 26-ZnO_{NT} (flow rate: 1.5×10^{-4} L min^{-1}) and 0.101 s for 10-ZnO_{NT} (flow rate: 1.0×10^{-4} L min^{-1}), respectively.

Regression analysis on R_{CT} value. In our published work,[1] corresponding to different ZnO_{NTs} reactors with pore sizes of 168, 96, 61, 26 and 10 nm, the average values of dimensionless R_{CT} were 3.15×10^{-6}, 7.33×10^{-6}, 12.14×10^{-6}, 24.34×10^{-6} and 80.2×10^{-6}, respectively. As shown in Equation (S3), non-linear regression analysis revealed that the R_{CT} value exponentially enhanced as a function of decreasing nanoreactor size ($d_{ZnO_{NT}}$), with correlation coefficient in a relative high level ($R^2 > 0.96$).

$$R_{CT} = [7.1 + 78.5 * exp(-\frac{d_{ZnO_{NT}} - 9.2}{11.4})] * 10^{-6} \qquad (10 \leq d_{ZnO_{NT}} \leq 168)$$
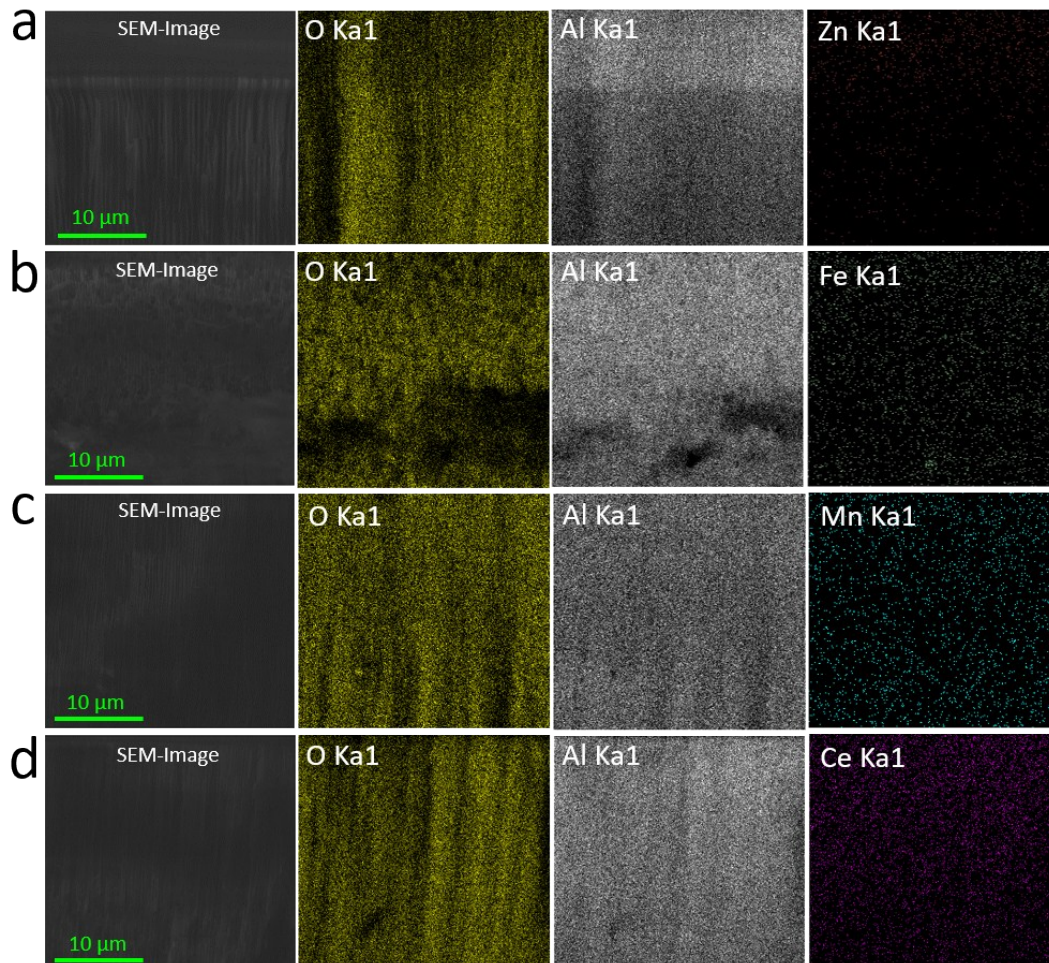
(S3)

Fig. S1 SEM-EDS mapping analysis of AAO-templated (a) zinc oxide nanotubes, (b) iron oxide nanoplates, (c) manganese oxide nanoparticles, and (d) cerium oxide nanobranches.
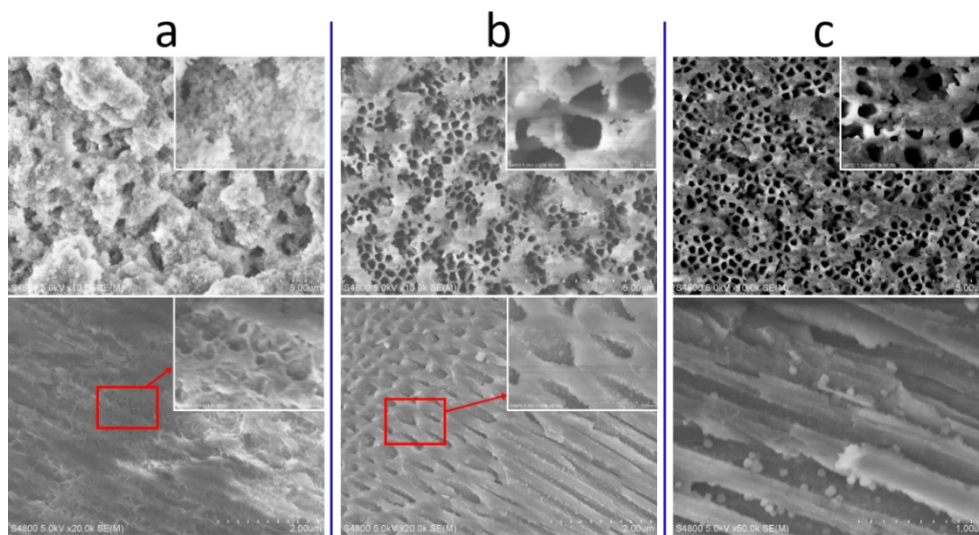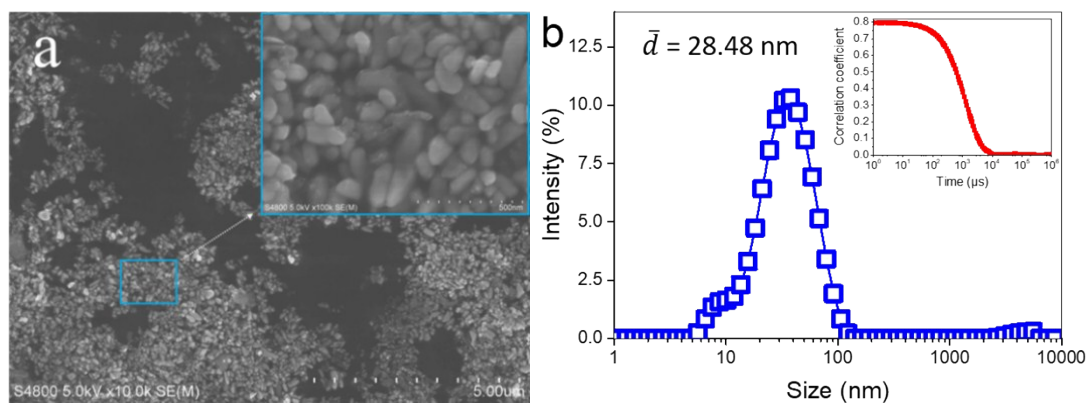
Fig. S3 (a) SEM images and (b) size distribution of zinc oxide nanoparticles (ZnO$_{NP}$).
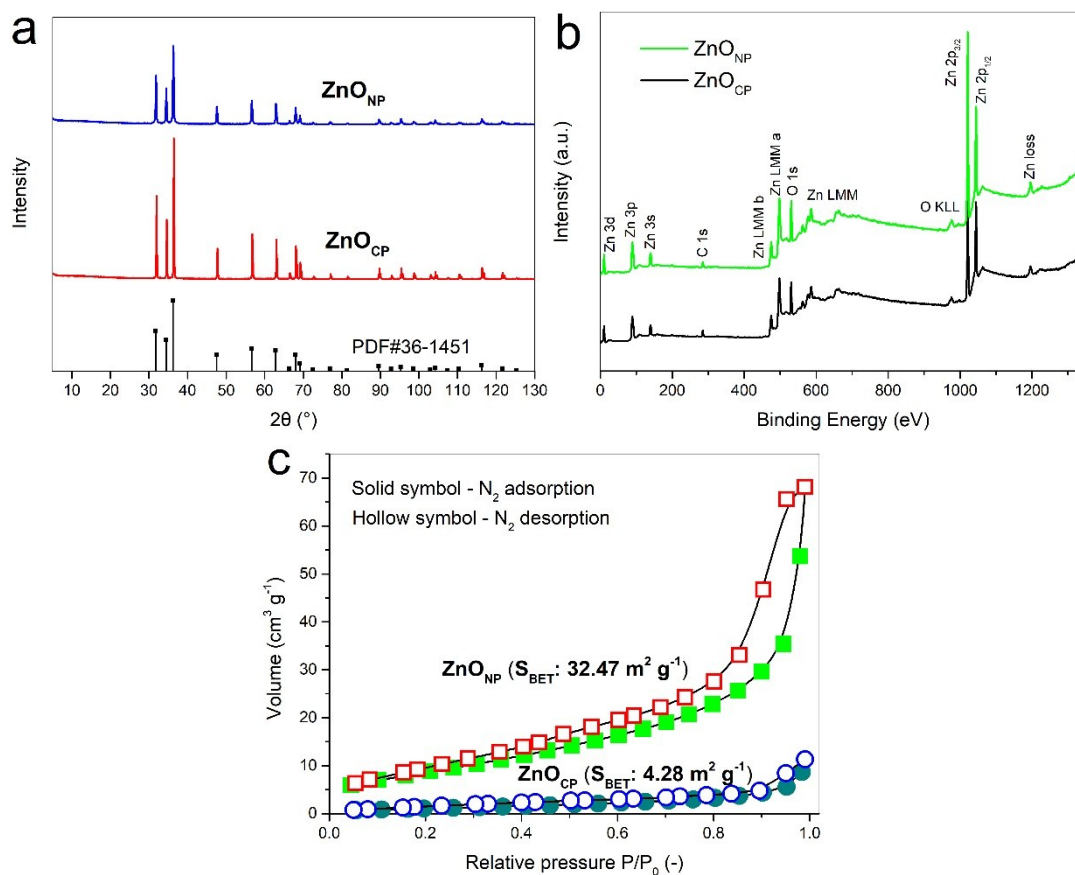

Fig. S4 (a) XRD patterns, (b) XPS spectra, and (c) nitrogen adsorption/desorption isotherms for

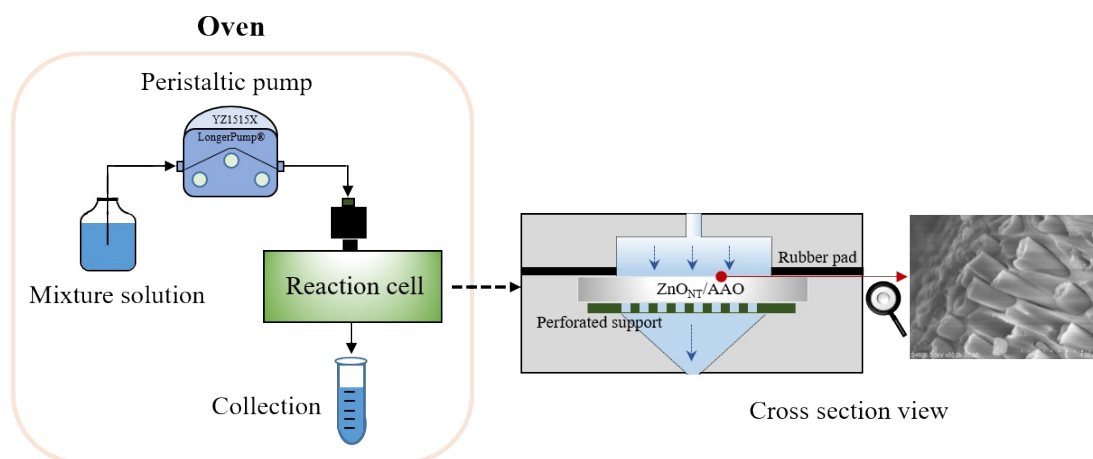as-synthesized ZnO$_{NP}$ and commercial ZnO$_{CP}$, respectively.

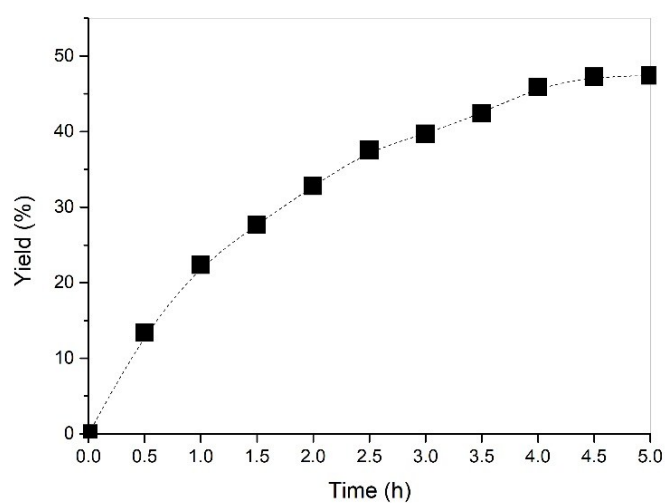**Fig. S5** Schematic illustration of the flow-through system used for catalytic condensation.

Fig. S6 Yield of BM versus time for Knoevenagel condensation in the presence of ZnO_{NP}.

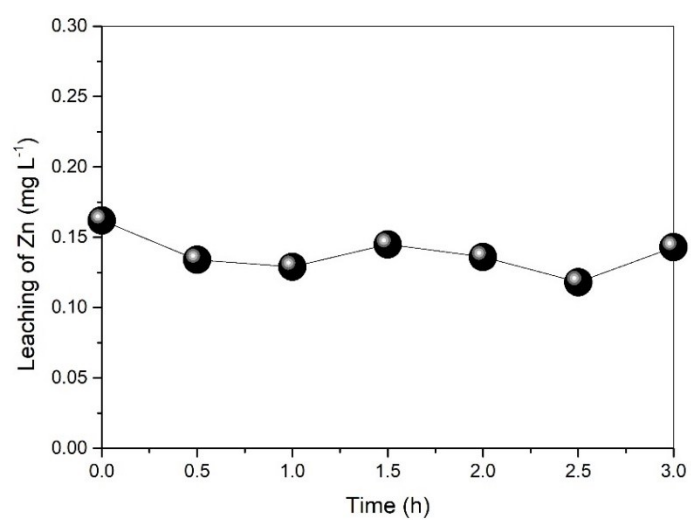Condition: temperature, 60 °C; solid load, 4 g L^{-1}.

Fig. S7 Leaching of Zn during ZnO_{NT}-induced catalytic condensation.

Condition: temperature, 60 °C; liquid flux, 0.5 mL min^{-1}.

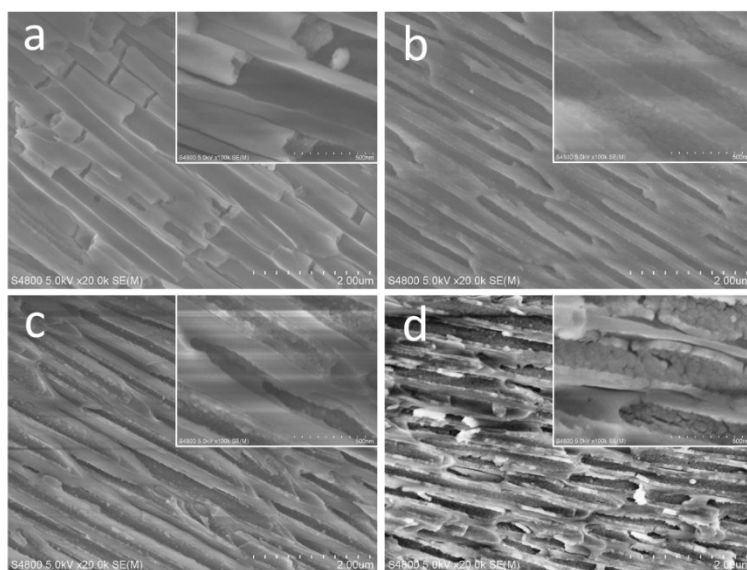**Fig. S8** Cross-section view of ZnO_{NT}/AAO after (a) 0 h, (b) 1 h, (c) 3 h and (d) 5 h reactions, respectively. Conditions: ZnO_{NT}, 168 nm pore; liquid flux, 0.5×10^{-3} L min^{-1}; temperature, 60 °C.
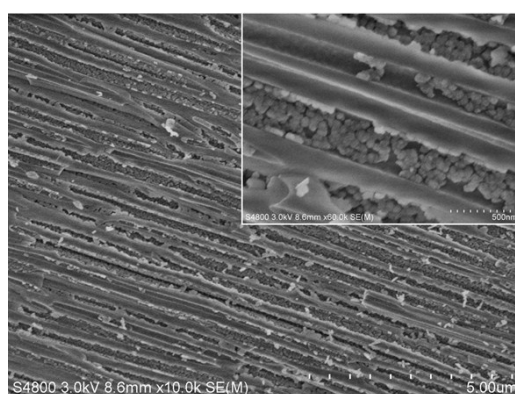

Fig. S9 Cross-section view of ZnO_{NT}/AAO after 5 h flow-through reaction. Conditions: ZnO_{NT}, 168 nm pore; liquid flux, 2.5×10^{-3} L min^{-1}; temperature, 60 °C.

Table S1 Comparison of ZnO_{NT} nanoreactors with reported batch reactors[2] in conversion of benzylidenemalononitrile through Knoevenagel condensation of benzaldehyde with malononitrile.

Catalyst	Description	Mode	Temp. (℃)	solvent	Yield (%)	Time (min)	Rate[a] (% s^{-1})	Ref.
ZnO_{NT}	arrayed nanotubes	Nano-reactor	60	ethanol	5.5-10.4	1.7×10^{-3} -10^{-2}	17.0-54.5	This work
ZnO_{NP}	nanoparticles	Batch reactor	60	ethanol	47	300	2.61×10^{-3}	This work
ZnO	powdered precipitates	Id.	room	-	92	80	1.9×10^{-2}	a
NF-ZnO	nanoflakes	Id.	25	-	90	210	7.1×10^{-3}	b
NaYN-850	ammonia-nitridated NaY zeolite	Id.	80	toluene	90	180	8.3×10^{-3}	c
BZN30024	nitridation of zeolite beta at 300℃	Id.	80	toluene	93	15	0.1	d
LZSM-5-AT−OH⁻	ammonia-modified ZSM-5 zeolite	Id.	80	toluene	92.6	60	2.6×10^{-2}	e
ZIF-8	Zn-incorporated zeolitic imidazolate framework	Id.	20	toluene	60	240	4.2×10^{-3}	f
Fe-MIL-101-NH$_2$	iron-containing MOF	Id.	80	toluene	78	30	4.3×10^{-2}	g
{[Lu(BTC)(H$_2$O)]·DMF}$_n$	needle-shaped Lu(III)-MOF	Id.	100	p-xylene	57	480	2.0×10^{-3}	h
ABIL@HKUST-1/Ethanol	amino-functionalized hybrid MOF	Id.	30	toluene	100	210	7.9×10^{-3}	i
CAU-1-NH$_2$	Al-based MOF with amino groups	Id.	40	ethanol	94	60	2.6×10^{-2}	j
UiO-66-NH$_2$	amino-functionalized Zr(IV)-MOF	Id.	40	DMF	98	40	4.1×10^{-2}	k
NH$_2$(50%)-MIL-53(Al)	amino-based MOF	Id.	80	DMF	99	300	5.5×10^{-3}	l
N-GO-1.00	amine grafted graphene oxide	Id.	40	decane/CH$_3$CN	96.5	240	6.7×10^{-3}	m
Chitosan	purchased solid base catalyst	Id.	40	ethanol	98	60	2.7×10^{-2}	n
MPB	magnetic polymer brushes	Id.	NA	tetrahydrofuran	99.4	480	3.5×10^{-3}	o
RhPt/TC@GO	monodisperse rhodium/platinum nanoparticles	Id.	room	water/methanol	＞99	10	＞0.17	p
Pd/AlO(OH)	commercial composite nanoparticles	Id.	room	water/methanol	85	25	5.7×10^{-2}	q
Fe$_3$O$_4$@SiO$_2$@Ni-Zn-Fe LDH	magnetic layered double hydroxide	Id.	60-70	ethanol	85	40	3.5×10^{-2}	r

[a] A quick back calculation of the average value according to the reported yield of product and time spent for catalysis.

References

1   S. Zhang, X. Quan, D. Wang, *Environ. Sci. Technol.* 2018, **52**, 8701-8711.

2   (a) M. Basude, P. Sunkara, V. S. Puppala, *J. Chem. Pharm. Res.* 2013, **5**, 46-50; (b) M. Hosseini-Sarvari, H. Sharghi, S. Etemad, *Helv. Chim. Acta* 2008, **91**, 715-724; (c) S. Ernst, M. Hartmann, S. Sauerbeck, T. Bongers, *Appl. Catal. A-Gen.* 2000, **200**, 117-123; (d) K. Narasimharao, M. Hartmann, H. H. Thiel, S. Ernst, *Micropor. Mesopor. Mat.* 2006, **90**, 377-383; (e) L. Xu, C. Li, K. Zhang, P. Wu, *ACS Catal.* 2014, **4**, 2959-2968; (f) H. Y. Cho, J. Kim, S. N. Kim, W. S. Ahn, *Micropor. Mesopor. Mat.* 2013, **169**, 180-184; (g) M. Hartmann, M. Fischer, *Micropor. Mesopor. Mat.* 2012, **164**, 38-43; (h) M. Almáši, V. Zeleňák, M. Opanasenko, I. Císařová, *Catal. Today* 2015, **243**, 184-194; (i) Q. Luo, B. An, M. Ji, S. E. Park, C. Hao, Y. Li, *J. Porous Mater.* 2015, **22**, 247-259; (j) A. Dhakshinamoorthy, N. Heidenreich, D. Lenzen, N. Stock, *CrystEngComm* 2017, **19**, 4187-4193; (k) Y. Yang, H. F. Yao, F. G. Xi, E. Q. Gao, *J. Mol. Catal. A-Chem.* 2014, **390**, 198-205; (l) F. Martínez, G. Orcajo, D. Briones, P. Leo, G. Calleja, *Micropor. Mesopor. Mat.* 2017, **246**, 43-50; (m) B. Xue, J. Zhu, N. Liu, Y. Li, *Catal. Commun.* 2015, **64**, 105-109; (n) B. Sakthivel, A. Dhakshinamoorthy, *J. Colloid. Interf. Sci.* 2017, **485**, 75-80; (o) C. S. Gill, W. Long, C. W. Jones, *Catal. Lett.* 2009, **131**, 425-431; (p) B. Şen, E. H. Akdere, A. Şavk, E. Gültekin, Ö. Paralı, H. Göksu, F. Şen, *Appl. Catal. B-Environ.* 2018, **225**, 148-153; (q) H. Göksu, E. Gültekin, *ChemistrySelect* 2017, **2**, 458-463; (r) M. Gilanizadeh, B. Zeynizadeh, *New J. Chem.* 2018, **42**, 8553-8566.